

Contents lists available at ScienceDirect

Colloids and Surfaces A: Physicochemical and Engineering Aspects

journal homepage: www.elsevier.com/locate/colsurfa





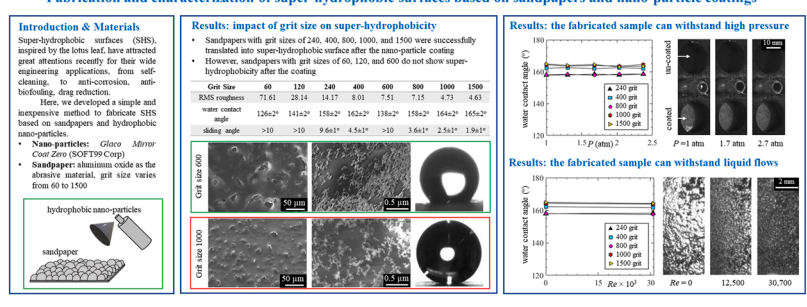
Fabrication and characterization of super-hydrophobic surfaces based on sandpapers and nano-particle coatings

Shabnam Mohammadshahi, Jordan Breveleri, Hangjian Ling

Department of Mechanical Engineering, University of Massachusetts Dartmouth, Dartmouth, MA 02747, USA

G R A P H I C A L A B S T R A C T

Fabrication and characterization of super-hydrophobic surfaces based on sandpapers and nano-particle coatings



ARTICLE INFO

Keywords: Superhydrophobic surface Sandpaper Plastron stability

ABSTRACT

In this work, we fabricate a series of super-hydrophobic surfaces by sprayed-coating a layer of hydrophobic nanoparticles on sandpapers that contain micro-scale abrasive particles. Sandpapers with a range of grit sizes from 60 to 1500 are investigated. We find that the coated sandpaper with grit sizes of 240, 400, 800, 1000, and 1500 exhibit super-hydrophobicity with a high water contact angle ranging from 158° to 165° and a low sliding angle varying from 10° to 2° . However, other coated sandpapers with grit sizes of 60, 120, and 600 do not show superhydrophobicity, possibly for the reason that the Cassie-Baxter state is not stable. Furthermore, we study the impacts of hydrostatic pressure and liquid flow on the robustness of the super-hydrophobic sandpapers. We find that the percentage of surface area covered by gas reduces due to pressure and liquid flow as expected, but the samples remain in the partial Cassie-Baxter state at the highest pressure (2.4 atm) and highest flow speed (5.0 m/s). After the pressure and flow tests, all samples retain their super-hydrophobic properties. The robustness of the air plastron on the fabricated samples could be attributed to the hierarchical roughness structures. In conclusion, we develop a method that could significantly reduce the cost of fabricating robust super-hydrophobic surfaces. Future work is required to evaluate the performance of the super-hydrophobic sandpapers for applications such as drag reduction, anti-biofouling, and anti-icing.

E-mail address: hling1@umassd.edu (H. Ling).

^{*} Corresponding author.

1. Introduction

Super-hydrophobic surfaces (SHS), initially inspired by the unique water-repellent characteristics of the lotus leaf [1] and animal skins [2, 3], have a large water contact angle ($>150^{\circ}$) and a small sliding angle ($<10^{\circ}$) [4]. The SHS has self-cleaning properties as droplets of water move along such surfaces, roll, and collect dust and particulates. When contacting with water, the SHS traps a layer of air bubbles (or plastron) between the surface roughness, forming the so-called Cassie-Baxter state [5]. Because of its unique properties, the SHS has found applications in many areas, from self-cleaning applications [6,7] to protecting materials from corrosion [8,9] and biofouling [10,11], separating oil and water [12,13], enhancing heat and mass transfer [14–16], and reducing the hydrodynamic skin-friction drag [17–20]. However, a wetting transition could occur when the air on SHS is removed due to pressure [21–24], liquid flows [25–27], and gas dissolution [28–30], limiting the application of SHS in many underwater systems.

During the last two decades, a range of fabrication technologies has been developed to create SHS. The fabrication methods have been reviewed by many authors [31–33]. Creating SHS typically follows two steps: (i) creating micro/nano-scale surface roughness, and (ii) functionalizing the surface with low surface energy. Surface roughness has been created by technologies such as photolithography [34], laser texturing [35-37], chemical etching [38], sandblasting [39-41], sprayed coating [19], dip coating [42], sol-gel method [43], etc. Both well-organized textures (such as posts, holes, and ridges) [44], and randomly roughed surfaces have been fabricated. The texture size can range from a few nanometers [45] to hundreds of micrometers [46]. Low surface energy can be achieved by either depositing a monolayer of hydrophobic material (e.g., highly fluorinated silanes) on top of the rough surface [47], or by spraying hydrophobic micro/nano-particles to a smooth surface [48], or by creating roughness on a hydrophobic surface [49].

In this paper, we aim to develop a simple and inexpensive method to fabricate SHS by taking advantage of the widely used sandpaper. Sandpaper includes a range of abrasive particles with a size on the order of 10–100 μm , depending on the grit size of the sandpaper. There are two main advantages of using sandpaper to create SHS. First, one key step for the fabrication of SHS is to create surface roughness. Sandpaper is a surface with inherent surface roughness formed by abrasive particles. By design, these abrasive particles firmly attach to the surface, ensuring the robustness of the surface roughness. More importantly, sandpaper is widely used in the industry and is very cheap to fabricate. Thus, by taking advantage of the surface roughness on the sandpaper, one can develop a simple, inexpensive, and robust method to create SHS. Secondly, by modifying the grit (or mesh) sizes of the sandpaper, one can optimize the surface texture of the SHS and achieve the best SHS performance. For example, SHS with a larger drag reduction is expected to be achieved by selecting sandpapers with smaller grit sizes (i.e., larger texture wavelength) [50]. On the other hand, SHS that can withstand higher pressures is obtained by using sandpapers with larger grit sizes (i. e., smaller texture wavelength) [21].

Despite many advantages including the low costs of using sandpapers to create surface roughness on SHS, no studies have fabricated SHS directly on top of sandpapers [51]. Therefore, this work has three aims: (1) demonstrate whether the sandpapers can be turned into SHS by depositing a low surface energy material on top; (2) investigate the impact of the grit size of sandpaper on the resulting water contact angle; and (3) study the robustness of fabricated SHS under liquid flows and pressure. We sprayed hydrophobic nano-particles on top of the sandpaper and characterized their hydrophobicity. The hydrophobic nano-particles served two purposes: alter the surface energy and create additional nano-scale surface roughness. We tested various sandpapers with grit sizes ranging from 60 to 1500. By measuring the water contact angle and sliding angle, we will show that most coated sandpapers do exhibit super-hydrophobic properties. Furthermore, we studied the

impacts of hydrostatic pressure and liquid flow on the robustness of the super-hydrophobic properties, and found the fabricated samples are suitable for underwater applications.

2. Materials and methods

A series of super-hydrophobic surfaces were fabricated by spray coating a layer of hydrophobic nano-particles on commercially available sandpapers. The hydrophobic nano-particles are 30-50 nm silanized silica particles from a commercial product: Glaco Mirror Coat Zero (SOFT99 Corp). Before spraying these particles are dispersed uniformly in an isopropyl alcohol solution. After spraying, the solvent quickly evaporates, leaving only the nano-particles on the surface. These hydrophobic nano-particles were previously used in other studies [52–56] to produce SHS. The sandpapers involved in this study have aluminum oxide as the abrasive material and have a grit size ranging from 60 to 1500. Before spraying the nano-particles, the sandpapers were first cleaned in an ultrasonic bath, dried, and firmly attached to a flat plate to ensure the flatness. Then, the nano-particles were sprayed over the entire sandpaper. Finally, the sample was allowed to dry in ambient air for one day for later experiments. As recommended by the manufacturer, during the spraying process, the pressurized container which stored the hydrophobic nano-particles was kept at a distance of 15 cm away from sandpaper. We sprayed the solution from side-to-side and top-to-bottom to ensure that the hydrophobic nano-particles were evenly distributed over the entire sandpapers.

The surface morphology of the samples was examined by scanning electron microscopy (SEM) (Hitachi SU-5000 field emission SEM). From the SEM images, we estimated the size (d) and wavelength (λ) of the abrasive particles on the sandpaper. We manually selected the centroids of individual abrasive particles on the SEM images. The wavelength was defined as the separation distance between the centroids of two adjacent particles. We randomly selected at least 20 pairs of adjacent particles and measured their separation distances as well as their sizes. The mean values and standard deviations were reported in this study. The surface roughness including root-mean-square roughness height (R_{rms}) and skewness (s) was characterized by a surface profiler (Bruker DektakXTTM stylus), which has a resolution of $0.1~\mu m$ in the wall-normal direction. Water contact angles and sliding angles are measured using the sessile droplet method. All the measurements were taken at three different positions on the same sample and the averaged results were reported.

We examined the impacts of hydrostatic pressure and liquid flow on the stability of the air layer as well as the durability of superhydrophobic properties on the fabricated samples. In the pressure test, the sample was installed in a closed tank filled with water. The pressure in the tank varied from 1.0 to 2.4 atm and was monitored by a highprecision pressure gauge. In the flow test, the sample was installed in a closed loop, recirculating channel flow facility. The flow facility has a test section with a dimension of 1016 mm \times 50 mm \times 6.4 mm (length \times width \times height), and a mean flow speed ranging from 0.5 to 5.0 m/s. The Reynolds number based on channel height and mean flow speed, Rem, varies from 3200 to 30,700. The sample was installed at 710 mm downstream from the entrance of the channel, so that the flow above the sample was fully developed. In all experiments, DI water was used. Prior to the experiments, the DI water was exposed to air at atmospheric pressure for more than 2 days. This ensured that the water was saturated with air at atmospheric pressure [57].

To examine the stability of the air layer, we used optical imaging based on Total Internal Reflection (TIR), a technology frequently used in the literature [2,58–61]. A CMOS camera (FLIR, model #GS3-U3–41C6M-C, 2048 \times 2048 pixels, 5.5 μm pixel size) and a LED light source were used for the TIR imaging. The incident angle of light rays was greater than the critical angle (48°) for the occurrence of total internal reflection at the water/air interface. Thus, the surface areas covered by the air appeared bright in the image, while those exposed to water were dark. To quantify the durability of super-hydrophobic

properties against high pressure or liquid flow, we run the experiment at the desired condition for 10 min, and then took the sample out from the facility, exposed it to the atmosphere, and measured the water contact angle immediately after the tests.

We also tried a different type of super-hydrophobic coating (Ultra-Ever Dry, UltraTech International, Inc, US) on the same sandpapers. The application of UltraEver Dry coating typically involves two steps: a bottom coat for generating surface roughness, and a top-coat for altering the surface hydrophobic chemistry. Since the sandpapers themselves have surface roughness, we only applied the UltraEver Dry Top Coat on the sandpapers. We found that both Glaco Mirror Coat Zero and UltraEver Dry Top Coat do not alter the surface roughness of the original sandpapers, and the resulting water contact angles are nearly the same (Supplementary Table 1). In the following, we only report results for sandpapers coated by Glaco Mirror Coat Zero. We did not synthesize hydrophobic coatings ourselves for the reason that the main purpose of this study is to demonstrate whether sandpapers could be turned into super-hydrophobic surfaces. We expect that using a self-prepared hydrophobic coatings, e.g., by following a method developed in [62] titanium dioxide nano-particles coated with fluorooctyltriethoxysilane were created, would produce similar results.

3. Results and discussion

The magnitudes of R_{rms} , s, d, and λ for the coated sandpaper with all grit sizes tested in this study ranging from 60 to 1500 are provided in Table 1. SEM images of coated sandpaper with all grit sizes are shown in Fig. 1. As expected, all samples are covered by a combination of microscale abrasive particles originally from the sandpaper and nano-scale roughness due to the application of hydrophobic nano-particles. As increasing the grit size from 60 to 1500, the size of the abrasive particles (d) estimated from these SEM images reduces from 218 μ m to 6 μ m, and the magnitude of R_{rms} reduces from 72 μ m to 4.6 μ m. We also measured the values of R_{rms} for un-coated sandpaper and found that R_{rms} for coated sandpaper is only about 0.3 μ m larger than R_{rms} for un-coated sandpaper (Supplementary Table 2). The values of R_{rms} are consistent with those reported in previous studies [63]. The impact of nano-particles on the modification of roughness height also agrees with previous works [55, 641].

The magnitudes of the water contact angle (WCA) and sliding angle are also listed in Table 1. Interestingly, the coated sandpapers with grit sizes of 240, 400, 800, 1000, and 1500 do exhibit the super-hydrophobic properties, including a high WCA larger than 150° and a small sliding angle lower than 10°. However, the coated sandpapers with grit sizes of 60, 120, and 600 show no super-hydrophobic properties. Although all coated sandpapers have the same chemical composition, they have different WCAs for the reason that their texture geometries are different. As shown in Fig. 2(a), reducing the abrasive particle size (i.e., increasing the grit size) generally leads to a larger WCA, except for the sandpaper

with a grit size of 600. This is probably because when reducing the particle size, the gap between particles also reduces, and the surface can withstand a larger hydrostatic pressure and promotes a more stable Cassie-Baxter state.

Assuming all the coated sandpapers promote a Cassie-Baxter state when contacting with the liquid, the water contact angle can be estimated from the following equation [5]:

$$\cos\theta_{CB} = \phi_s \cos\theta_0 - 1 + \phi_s \tag{1}$$

where ϕ_s is the solid fraction (surface area covered by solid), θ_{CB} and θ_0 are the water contact angles on the rough sample and on an ideally flat surface of the same material. Assuming the coated sandpapers as regular circular posts (thus $\phi_s = \pi d^2/\lambda^2/4$) and $\theta_0 = 120^\circ$, we estimated the values of θ_{CB} and listed them in Table 1. Clearly, for coated sandpapers with grit sizes of 240, 400, 800, 1000, and 1500, the Cassie-Baxter model slightly under-predicts the WCA, probably because we didn't account the effect of nano-scale roughness in the model. For coated sandpapers with grit sizes of 60, 120, and 600, the model greatly over-predicts the WCA, indicating that these samples do not promote a Cassie-Baxter state.

To explain why coated sandpapers of grit sizes 60, 120, and 600 do not obtain super-hydrophobicity, we estimated the critical pressure for a wetting transition. The critical pressure p_c is the maximum pressure difference across the gas-liquid interface calculated from the force-balance equation as [21]:

$$\gamma \operatorname{L|cos}\theta_{ady}| = p_c(1 - \phi_s)\lambda^2 \tag{2}$$

where $\gamma=72\times10^{-3}$ N/m is the surface tension of water, L is the perimeter of the micro-textures cross-section, θ_{adv} is the local advancing contact angle on the side wall of the micro-textures, and λ is the texture wavelength. A wetting transition occurs when the pressure difference across the interface is larger than p_c . Surface textures with a larger p_c have a more stable Cassie-Baxter state. Assuming the coated sandpapers as regular circular posts and $\theta_{adv}=150^\circ$ (due to the nano-particles) [29], we calculated p_c and listed the results in Table 1. We found that the coated sandpapers showing no super-hydrophobicity have the lowest p_c .

To further estimate the stability of Cassie-Baxter state, we calculated the free-surface-energy difference between Wenzel state and Cassie-Baxter state. By considering interfacial energies only, the difference of free energy between Wenzel and Cassie-Baxter states per surface area *A* can be calculated as [65]:

$$\Delta E = (E^{Wezel} - E^{Cassie}) / A = \left[\; (\varphi_s - r_W) \; cos\theta_0 - 1 \; + \varphi_s \right] \gamma \eqno(3)$$

where r_W is the Wenzel roughness (the ratio of total surface area to project surface area). Assuming the coated sandpaper as regular circular posts with roughness height $H=R_{rms}$ (thus $r_W=1+\pi dH/\lambda^2$, ignoring the contribution of nano-scale roughness on r_W) and $\theta_0=120^\circ$, we calculated $\Delta E/\gamma$ and listed the results in Table 1. Clearly, the coated sandpapers showing no super-hydrophobicity have the lowest ΔE . Therefore,

Table 1
Parameters of coated sandpapers with grit sizes ranging from 60 to 1500, including rms roughness height (R_{rms}), skewness of roughness height (s), abrasive particles size (d), wavelength of the abrasive particles (λ), measured water contact angles (WCA), water contact angle predicted by Cassie-Baxter model (θ_{CB}), sliding angles, gas fraction (φ_g), critical pressure (p_c), and free-energy-difference (ΔE) between Wenzel state and Cassie-Baxter state. For d and λ , the mean values and standard devirations were listed in the table.

Grit Size	60	120	240	400	600	800	1000	1500
R _{rms} (µm)	71.61	28.14	14.17	8.01	7.51	7.15	4.73	4.63
S	0.48	0.91	0.05	0.05	0.51	0.1	0.2	0.06
d (μm)	218 ± 37	75 ± 26	42 ± 11	18 ± 10	23 ± 13	17 ± 6	10 ± 5	6 ± 3
λ (μm)	438 ± 80	167 ± 52	67 ± 14	28 ± 3	70 ± 20	33 ± 9	24 ± 8	12 ± 2
WCA	$126\pm2^{\circ}$	$141\pm2^\circ$	$158\pm2^{\circ}$	$162\pm2^{\circ}$	$138\pm2^{\circ}$	$158\pm2^{\circ}$	$164\pm2^{\circ}$	$165\pm2^{\circ}$
θ_{CB}	154°	157°	148°	146°	163°	154°	159°	154°
Sliding angle	$>10^{\circ}$	> 10	$9.6\pm1^{\circ}$	$4.5\pm1^{\circ}$	$>10^{\circ}$	$3.6\pm1^{\circ}$	$2.5\pm1^{\circ}$	$1.9\pm1^{\circ}$
Gas fraction φ_g	0.021	0.032	0.68	0.86	0.56	0.85	0.93	0.932
p_c (Pa)	276	626	2649	6654	1004	3861	4638	10,150
$\Delta E/\gamma$	-0.15	-0.18	0.07	0.24	-0.35	-0.05	-0.11	0.2

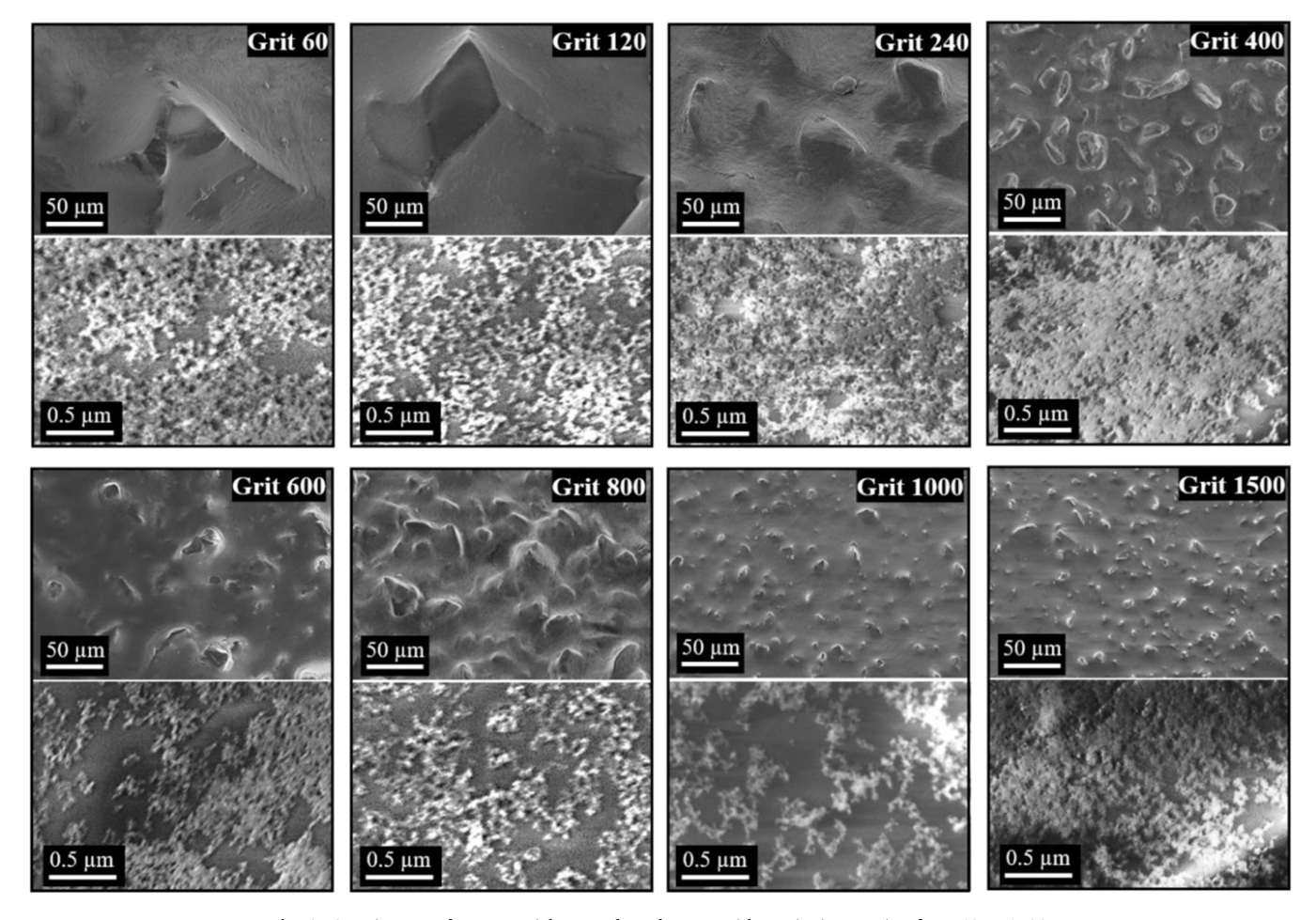


Fig. 1. SEM images of nano-particle coated sandpapers with a grit size ranging from 60 to 1500.

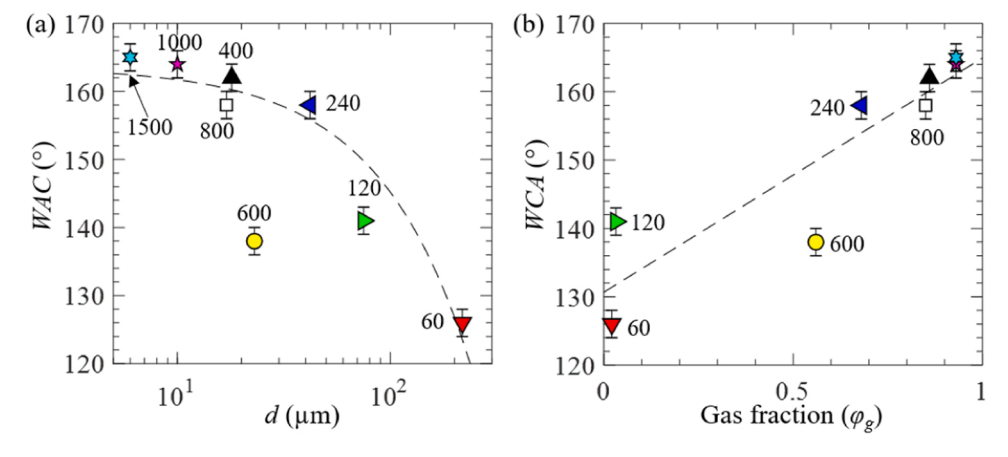


Fig. 2. Water contact angle as a function of abrasive particle size (a) and gas fraction (b). The numbers against the symbols are the grit sizes of the sandpapers.

based on the analysis of p_c and ΔE , the possible reason that certain coated sandpapers showing no super-hydrophobicity is because the Cassie-Baxter state is not stable.

The status of air layer on coated sandpapers when the samples are fully immersed in water is shown in Fig. 3. It can be seen that all the coated sandpapers are partially covered by the air. From these images, we estimated the percentage of surface area covered by air (i.e., gas fraction φ_g), and the results are provided in Table 1. The magnitude of φ_g varies from 0.02 to 0.93. Fig. 2(b) shows the contact angle as a function of φ_g . As expected, samples with a higher φ_g have a higher WCA,

consistent with the Cassie-Baxter model in Eq. (1). The reason that sandpapers with grit sizes of 60, 120, and 600 have much lower gas fractions compared to others, as explained earlier, is due to the low stability of Cassie-Baxter state.

We then investigated the impact of hydrostatic pressure on the stability of the plastron and the durability of super-hydrophobicity of the coated sandpaper. We only studied samples that showed high water contact angles and low sliding angles, i.e., these samples with grit sizes of 240, 400, 800, 1000, and 1500. Fig. 4(a) compares the *WCA* before and after the pressure tests. The results show that the *WCA* remains

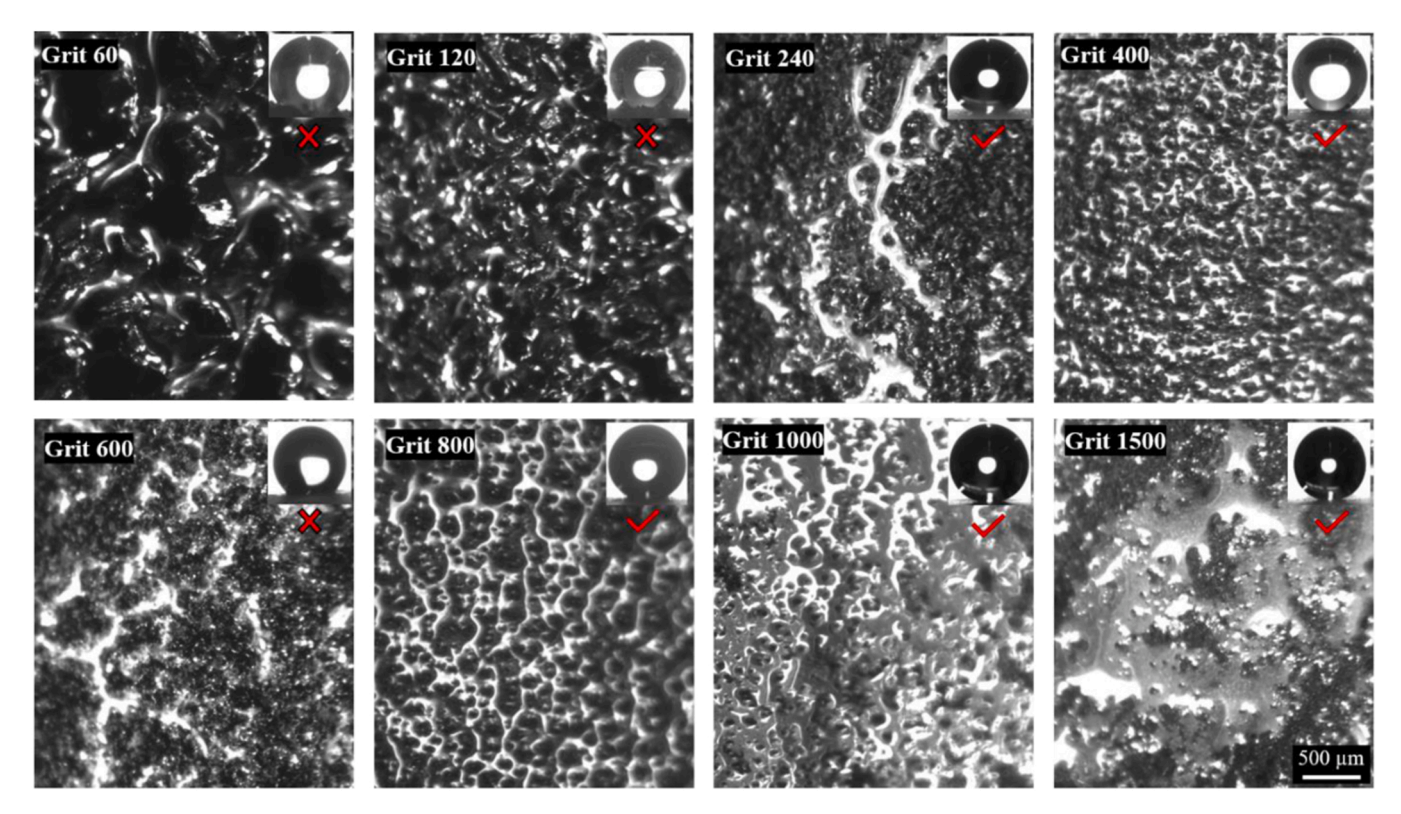


Fig. 3. Status of air layer on the coated sandpapers when the samples are fully immersed in water (at a water depth of 10 cm). Samples with grit sizes of 60, 120, and 600 do not show super-hydrophobicity and have relatively lower air fraction compared to these exhibiting super-hydrophobicity.

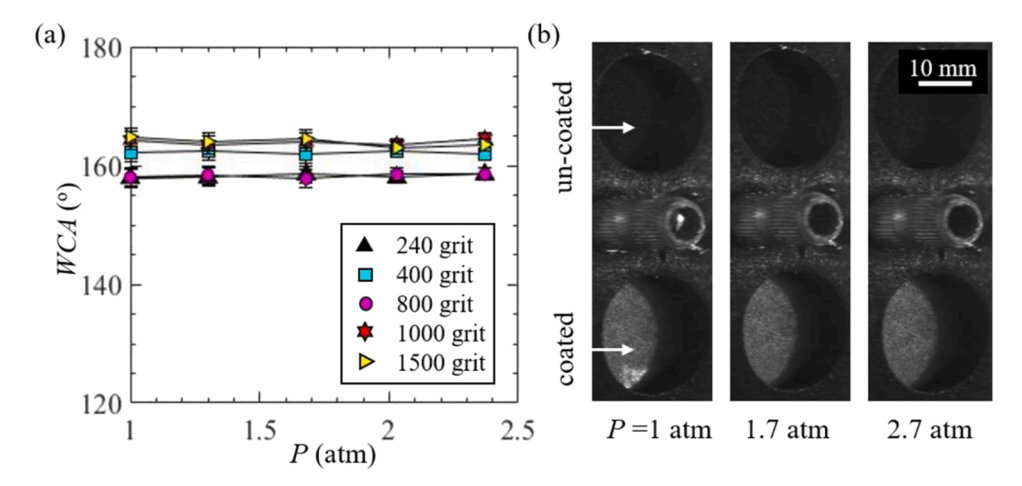


Fig. 4. (a) Water contact angles at different hydrostatic pressures *P* ranging from 1.0 to 2.4 atm for coated sandpapers; and (b) status of air layer on coated sandpaper with grit size of 800 (sample at the bottom) (an un-coated sandpaper is also shown for comparison).

nearly the same after the tests, indicating that the samples retain their super-hydrophobic property after the high pressures test (at least 2.4 atm). To explain this observation, we studied the status of the air layer on one coated sandpaper with grit size 800 under different pressures. The results are shown in Fig. 4(b). As expected, even under the highest pressure (2.4 atm), the air bubbles persist on the sample, indicating that a wetting transition does not occur. We expect that the status of the air layer on other super-hydrophobic sandpapers will follow similar trends. The reason that the air layer on the fabricated samples could withstand high pressure is partially because of the combination of micro and nano-scale surface roughness, i.e., the hierarchical structures [65–67].

Last, we studied the impacts of liquid flow on the stability of plastron and the durability of the super-hydrophobicity of the coated sandpapers.

Fig. 5(a) compares the WCA before and after the flow tests. The WCA remains nearly the same after the tests, indicating that the samples retain their super-hydrophobicity. To explain this observation, Fig. 5(b) shows the status of the air layer on a coated sandpaper (with grit size 800) at Reynolds numbers ranging from 0 to 30,700. Even under the highest flow speed, the surface is still covered by small-scale, isolated air bubbles, although the percentage of surface area covered by gas is reduced. These results prove that the super-hydrophobic sandpapers could retain their super-hydrophobicity after being exposed to high-speed flows. Again, this robustness could be attributed to the hierarchical surface roughness [66]. At the highest Reynolds number of 30, 700, the wall friction applied on the coated sandpaper is estimated as 56 Pa (assuming a 20 % drag reduction by SHS). Thus, our results suggest that the bonding strength between hydrophobic nano-particles and

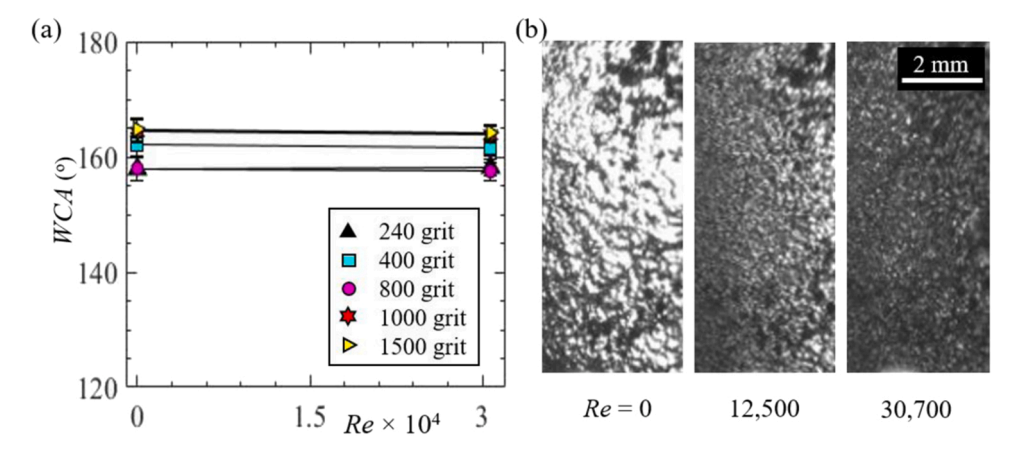


Fig. 5. (a) Water contact angles before and after flow tests under Reynolds numbers Re ranging from 0 and 30,700; and (b) status of air layer on coated sandpaper with grit size of 800 for Re from 0 to 30,700.

sandpaper is sufficient to retain the nano-particles in a liquid flow with a shear stress of 56 Pa.

4. Conclusions

In this study, we coated a number of sandpapers of different grit sizes with a layer of hydrophobic nano-particles, and characterized the coated sandpapers including the surface roughness, water contact angle, sliding angle, and gas fraction. We further measured the robustness of the superhydrophobic properties on the coated sandpapers under hydrostatic pressure and liquid flows. Our main conclusions are listed below:

- (1) We demonstrated that most sandpapers (grit sizes of 240, 400, 800, 1000, and 1500) can be turned into SHS by depositing a low surface energy material. Thus, our method significantly reduced the cost of fabricating SHS by taking advantage of the inherent surface roughness on sandpaper.
- (2) We found sandpapers with certain grit sizes (60, 120, and 600) did not show super-hydrophobicity probably due to the low stability of Cassie-Baxter state on these samples.
- (3) We found that the super-hydrophobic sandpapers maintained a partial Cassie-Baxter state under pressure and flows, and retained the super-hydrophobic properties after the pressure and flow tests. The robustness of the super-hydrophobic properties might be due to the hierarchical structures.

We expect that our method has applications in many areas such as drag reduction, anti-biofouling, and anti-icing. For example, the superhydrophobic sandpaper could be attached to underwater vessels to achieve drag reduction and energy saving. However, future studies are required to carefully evaluate the performance of the super-hydrophobic sandpapers in these applications. Future studies are also required to characterize as well as enhance the bonding strength between the hydrophobic nano-particles and sandpaper, which is critical for real-world applications.

CRediT authorship contribution statement

Shabnam Mohammadshahi: Data curation, Investigation, Formal analysis, Roles/Writing - original draft. **Jordan Breveleri:** Investigation. **Hangjian Ling:** Conceptualization, Funding acquisition, Supervision, Writing - review & editing.

Declaration of Competing Interest

The authors declare that they have no known competing financial interests or personal relationships that could have appeared to influence

the work reported in this paper.

Data availability

Data will be made available on request.

Acknowledgment

We thank the support of National Science Foundation under Grant No. 2041479, UMass Dartmouth's Marine and Undersea Technology (MUST) Research Program funded by the Office of Naval Research (ONR) under Grant No. N00014–20-1–2170, and Seed Funding program from the Office of the Provost at the University of Massachusetts Dartmouth.

Appendix A. Supporting information

Supplementary data associated with this article can be found in the online version at doi:10.1016/j.colsurfa.2023.131358.

References

- R.J. Daniello, N.E. Waterhouse, J.P. Rothstein, Drag reduction in turbulent flows over superhydrophobic surfaces, Phys. Fluids 21 (2009), https://doi.org/10.1063/ 1.3207885.
- [2] B.J. Lee, Z. Zhang, S. Baek, S. Kim, D. Kim, K. Yong, Bio-inspired dewetted surfaces based on SiC/Si interlocked structures for enhanced-underwater stability and regenerative-drag reduction capability, Sci. Rep. 6 (2016) 1–11, https://doi.org/ 10.1038/srep24653.
- [3] F. Van Breugel, M.H. Dickinson, J. Meinwald, Superhydrophobic diving flies (Ephydra hians) and the hypersaline waters of Mono Lake, Proc. Natl. Acad. Sci. USA 114 (2017) 13483–13488, https://doi.org/10.1073/pnas.1714874114.
- [4] F. Lin, L. Shuhong, L. Yingshun, L. Huanjun, Z. Lingjuan, S. Yanlin, L. Biqian, J. Lei, Z. Daoben, Super-hydrophobic surfaces: from natural to artificial, Adv. Mater. (2002) (https://onlinelibrary.wiley.com/doi/abs/10.1002/adma.200290020).
- [5] A.B.D. Cassie, S. Baxter, Wettability of porous surfaces, Trans. Faraday Soc. 40 (1944).
- [6] T. Kamegawa, Y. Shimizu, H. Yamashita, Superhydrophobic surfaces with photocatalytic self-cleaning properties by nanocomposite coating of TiO 2 and polytetrafluoroethylene, Adv. Mater. 24 (2012) 3697–3700, https://doi.org/ 10.1002/adma.201201037.
- [7] S.S. Latthe, P. Sudhagar, A. Devadoss, A.M. Kumar, S. Liu, C. Terashima, K. Nakata, A. Fujishim, Mechanically bendable superhydrophobic steel surface with its selfcleaning and corrosion-resistant properties, J. Mater. Chem. A 3 (2015) 10715–10722, https://doi.org/10.1039/b000000x.
- [8] J.F. Ou, X.Z. Fang, W.J. Zhao, S. Lei, M.S. Xue, F.J. Wang, C.Q. Li, Y.L. Lu, W. Li, Influence of hydrostatic pressure on the corrosion behavior of superhydrophobic surfaces on bare and oxidized aluminum substrates, Langmuir 34 (2018) 5807–5812, https://doi.org/10.1021/acs.langmuir.8b01100.
- [9] J. Ou, W. Hu, M. Xue, F. Wang, W. Li, Superhydrophobic surfaces on light alloy substrates fabricated by a versatile process and their corrosion protection, ACS Appl. Mater. Interfaces 5 (2013) 3101–3107, https://doi.org/10.1021/ prof/00124

- [10] A.M.A. Mohamed, A.M. Abdullah, N.A. Younan, Corrosion behavior of superhydrophobic surfaces: a review, Arab. J. Chem. 8 (2015) 749–765, https:// doi.org/10.1016/j.arabjc.2014.03.006.
- [11] G.B. Hwang, K. Page, A. Patir, S.P. Nair, E. Allan, I.P. Parkin, The anti-biofouling properties of superhydrophobic surfaces are short-lived, ACS Nano 12 (2018) 6050–6058, https://doi.org/10.1021/acsnano.8b02293.
- [12] K. Jayaramulu, K.K.R. Datta, C. Rösler, M. Petr, M. Otyepka, R. Zboril, R.A. Fischer, Biomimetic superhydrophobic/superoleophilic highly fluorinated graphene oxide and ZIF-8 composites for oil-water separation, Angew. Chem. - Int. Ed. 55 (2016) 1178–1182, https://doi.org/10.1002/anie.201507692.
- [13] H. Liu, J. Huang, Z. Chen, G. Chen, K.Q. Zhang, S.S. Al-Deyab, Y. Lai, Robust translucent superhydrophobic PDMS/PMMA film by facile one-step spray for selfcleaning and efficient emulsion separation, Chem. Eng. J. 330 (2017) 26–35, https://doi.org/10.1016/j.cej.2017.07.114.
- [14] P. Zhang, F.Y. Lv, A review of the recent advances in superhydrophobic surfaces and the emerging energy-related applications, Energy 82 (2015) 1068–1087, https://doi.org/10.1016/j.energy.2015.01.061.
- [15] M. Kharati-Koopaee, M.R. Akhtari, Numerical study of fluid flow and heat transfer phenomenon within microchannels comprising different superhydrophobic structures, Int. J. Therm. Sci. 124 (2018) 536–546, https://doi.org/10.1016/j. iithermalsci.2017.11.004.
- [16] Y. Cheng, J. Xu, Y. Sui, Numerical study on drag reduction and heat transfer enhancement in microchannels with superhydrophobic surfaces for electronic cooling, Appl. Therm. Eng. 88 (2015) 71–81, https://doi.org/10.1016/j. applthermaleng.2014.10.058.
- [17] J.P. Rothstein, Slip on superhydrophobic surfaces, Annu. Rev. Fluid Mech. 42 (2010) 89–109, https://doi.org/10.1146/annurev-fluid-121108-145558.
- [18] D. Song, R.J. Daniello, J.P. Rothstein, Drag reduction using superhydrophobic sanded Teflon surfaces, Exp. Fluids 55 (2014), https://doi.org/10.1007/s00348-014-1783-8
- [19] H. Ling, S. Srinivasan, K. Golovin, G.H. McKinley, A. Tuteja, J. Katz, High-resolution velocity measurement in the inner part of turbulent boundary layers over super-hydrophobic surfaces, J. Fluid Mech. 801 (2016) 670–703, https://doi.org/10.1017/ifm.2016.450.
- [20] H. Park, C.H. Choi, C.J. Kim, Superhydrophobic drag reduction in turbulent flows: a critical review, Exp. Fluids 62 (2021) 1–29, https://doi.org/10.1007/s00348-021.03322.4
- [21] Q.S. Zheng, Y. Yu, Z.H. Zhao, Effects of hydraulic pressure on the stability and transition of wetting modes of superhydrophobic surfaces, Langmuir 21 (2005) 12207–12212, https://doi.org/10.1021/la052054y.
- [22] L. Lei, H. Li, J. Shi, Y. Chen, Diffraction patterns of a water-submerged superhydrophobic grating under pressure, Langmuir 26 (2010) 3666–3669, https://doi.org/10.1021/la903150h.
- [23] C.W. Extrand, Repellency of the lotus leaf: resistance to water intrusion under hydrostatic pressure, Langmuir 27 (2011) 6920–6925, https://doi.org/10.1021/ 12010329
- [24] P. Papadopoulos, L. Mammen, X. Deng, D. Vollmer, H.-J. Butt, How superhydrophobicity breaks down, Proc. Natl. Acad. Sci. USA 110 (2013) 3254–3258. https://doi.org/10.1073/pnas.1218673110.
- [25] J. Hyväluoma, J. Harting, Slip flow over structured surfaces with entrapped microbubbles, Phys. Rev. Lett. 100 (2008), 246001, https://doi.org/10.1103/ PhysRevLett.100.246001.
- [26] P. Gao, J.J. Feng, Enhanced slip on a patterned substrate due to depinning of contact line, Phys. Fluids 21 (2009), 102102, https://doi.org/10.1063/1.325425.
- [27] B. Vajdi Hokmabad, S. Ghaemi, Turbulent flow over wetted and non-wetted superhydrophobic counterparts with random structure, Phys. Fluids 28 (2016), https://doi.org/10.1063/1.4940325.
- [28] Y. Xue, P. Lv, H. Lin, H. Duan, Underwater superhydrophobicity: stability, design and regulation, and applications, Appl. Mech. Rev. 68 (2016), https://doi.org/ 10.1115/1.4033706
- [29] H. Ling, J. Katz, M. Fu, M. Hultmark, Effect of Reynolds number and saturation level on gas diffusion in and out of a superhydrophobic surface, Phys. Rev. Fluids 2 (2017) 1–17, https://doi.org/10.1103/PhysRevFluids.2.124005.
- [30] S. Huang, P. Lv, H. Duan, Morphology evolution of liquid–gas interface on submerged solid structured surfaces, Extrem. Mech. Lett. 27 (2019) 34–51, https://doi.org/10.1016/j.eml.2019.01.005.
- [31] P. Roach, N.J. Shirtcliffe, M.I. Newton, Progess in superhydrophobic surface development, Soft Matter 4 (2008) 224, https://doi.org/10.1039/b712575p.
- [32] B. Bhushan, Y.C. Jung, Natural and biomimetic artificial surfaces for superhydrophobicity, self-cleaning, low adhesion, and drag reduction, Prog. Mater. Sci. 56 (2011) 1–108, https://doi.org/10.1016/j.pmatsci.2010.04.003.
- Y. Zhang, Z. Zhang, J. Yang, Y. Yue, H. Zhang, A review of recent advances in superhydrophobic surfaces and their applications in drag reduction and heat transfer, Nanomaterials 12 (2022), https://doi.org/10.3390/nano12010044.
 B. Cortese, S.D. Amone, M. Manca, I. Viola, R. Cingolani, G. Gigli,
- [34] B. Cortese, S.D. Amone, M. Manca, I. Viola, R. Cingolani, G. Gigli, Superhydrophobicity due to the hierarchical scale roughness, Langmuir (2008) 2712–2718
- [35] G. Feng, F. Li, W. Xue, K. Sun, H. Yang, Q. Pan, Y. Cao, Laser textured GFRP superhydrophobic surface as an underwater acoustic absorption metasurface, Appl. Surf. Sci. 463 (2019) 741–746, https://doi.org/10.1016/j.apsusc.2018.09.005.
- [36] Q. Ma, Z. Tong, W. Wang, G. Dong, Fabricating robust and repairable superhydrophobic surface on carbon steel by nanosecond laser texturing for corrosion protection, Appl. Surf. Sci. 455 (2018) 748–757, https://doi.org/ 10.1016/j.apsusc.2018.06.033.
- [37] H. Li, Y. Lai, J. Huang, Y. Tang, L. Yang, Z. Chen, K. Zhang, X. Wang, L.P. Tan, Multifunctional wettability patterns prepared by laser processing on

- superhydrophobic TiO2 nanostructured surfaces, J. Mater. Chem. B. 3 (2015) 342–347, https://doi.org/10.1039/c4tb01814a.
- [38] S. Hoshian, V. Jokinen, S. Franssila, Robust hybrid elastomer/metal-oxide superhydrophobic surfaces, Soft Matter 12 (2016) 6526–6535, https://doi.org/ 10.1039/c6sm01095d.
- [39] R. Sun, J. Zhao, Z. Li, J. Mo, Y. Pan, D. Luo, Preparation of mechanically durable superhydrophobic aluminum surface by sandblasting and chemical modification, Prog. Org. Coat. 133 (2019) 77–84, https://doi.org/10.1016/j. porgcoat.2019.04.020.
- [40] L. Li, J. Zhu, S. Zhi, E. Liu, G. Wang, Z. Zeng, W. Zhao, Q. Xue, Study of adhesion and friction drag on a rough hydrophobic surface: sandblasted aluminum, Phys. Fluids 30 (2018), https://doi.org/10.1063/1.5039712.
- [41] Z. Zhang, Z. Shen, H. Wu, L. Li, X. Fu, Study on preparation of superhydrophobic ni-co coating and corrosion resistance by sandblasting– electrodeposition, Coatings 10 (2020) 1–16, https://doi.org/10.3390/coatings10121164.
- [42] A.B. Gurav, Q. Xu, S.S. Latthe, R.S. Vhatkar, S. Liu, H. Yoon, S.S. Yoon, Superhydrophobic coatings prepared from methyl-modified silica particles using simple dip-coating method, Ceram. Int. 41 (2015) 3017–3023, https://doi.org/ 10.1016/j.ceramint.2014.10.137.
- [43] B. El Fouhaili, A. Ibrahim, C. Dietlin, A. Chemtob, X. Allonas, C. Croutxé-Barghorn, Single-step formation of superhydrophobic surfaces using photobase-catalyzed solgel process, Prog. Org. Coat. 137 (2019), 105293, https://doi.org/10.1016/j. porccoat.2019.105293.
- [44] A. Gaddam, H. Sharma, R. Ahuja, S. Dimov, S. Joshi, A. Agrawal, Hydrodynamic drag reduction of shear-thinning liquids in superhydrophobic textured microchannels, Microfluid. Nanofluidics 25 (2021) 1–19, https://doi.org/10.1007/ s10404-021-02470-7.
- [45] T.S. Wong, C.M. Ho, Dependence of macroscopic wetting on nanoscopic surface textures, Langmuir 25 (2009) 12851–12854, https://doi.org/10.1021/la902430w.
- [46] Z. Yang, C. Zhu, N. Zheng, D. Le, J. Zhou, Superhydrophobic surface preparation and wettability transition of titanium alloy with micro/nano hierarchical texture, Materials 11 (2018) 1–15, https://doi.org/10.3390/ma11112210.
- [47] T. Darmanin, G. Godeau, F. Guittard, Superhydrophobic, superoleophobic and underwater superoleophobic conducting polymer films, Surf. Innov. 6 (2018) 181–204, https://doi.org/10.1680/jsuin.18.00006.
- [48] J. Huang, P. Cai, M. Li, Q. Wu, Q. Li, S. Wang, Preparation of cnf/pdms superhydrophobic coatings with good abrasion resistance using a one-step spray method, Materials 13 (2020) 1–10, https://doi.org/10.3390/ma13235380.
- [49] Q. Wang, G. Sun, Q. Tong, W. Yang, W. Hao, Fluorine-free superhydrophobic coatings from polydimethylsiloxane for sustainable chemical engineering: preparation methods and applications, Chem. Eng. J. 426 (2021), 130829, https://doi.org/10.1016/j.cei.2021.130829
- [50] C. Lee, C.H. Choi, C.J. Kim, Superhydrophobic drag reduction in laminar flows: a critical review, Exp. Fluids 57 (2016) 1–20, https://doi.org/10.1007/s00348-016-2264-z.
- [51] Y. Qing, C. Long, K. An, C. Hu, C. Liu, Sandpaper as template for a robust superhydrophobic surface with self-cleaning and anti-snow/icing performances, J. Colloid Interface Sci. 548 (2019) 224–232, https://doi.org/10.1016/j. icis.2019.04.040.
- [52] I.U. Vakarelski, N.A. Patankar, J.O. Marston, D.Y.C. Chan, S.T. Thoroddsen, Stabilization of Leidenfrost vapour layer by textured superhydrophobic surfaces, Nature 489 (2012) 274–277, https://doi.org/10.1038/nature11418.
- [53] J. Zhang, Z. Yao, P. Hao, Drag reductions and the air-water interface stability of superhydrophobic surfaces in rectangular channel flow, Phys. Rev. E 94 (2016) 53117, https://doi.org/10.1103/PhysRevE.94.053117.
- [54] Y. Li, D. Quéré, C. Lv, Q. Zheng, Monostable superrepellent materials, Proc. Natl. Acad. Sci. USA 114 (2017) 3387–3392, https://doi.org/10.1073/ pnas 1614667114
- [55] A. Rajappan, K. Golovin, B. Tobelmann, V. Pillutla, W. Abhijeet, A. Choi, G. H. Tuteja, Mckinley, Influence of textural statistics on drag reduction by scalable, randomly rough superhydrophobic surfaces in turbulent flow, Phys. Fluids 31 (2019). https://doi.org/10.1063/1.5090514.
- [56] A. Rajappan, G.H. McKinley, Cooperative drag reduction in turbulent flows using polymer additives and superhydrophobic walls, Phys. Rev. Fluids 5 (2020), 114601, https://doi.org/10.1103/PhysRevFluids.5.114601.
- [57] P. Lv, Y. Xue, Y. Shi, H. Lin, H. Duan, Metastable states and wetting transition of submerged superhydrophobic structures, Phys. Rev. Lett. 112 (2014) 1–5, https:// doi.org/10.1103/PhysRevLett.112.196101.
- [58] M.S. Bobji, S.V. Kumar, A. Asthana, R.N. Govardhan, Underwater sustainability of the "Cassie" state of wetting, Langmuir 25 (2009) 12120–12126, https://doi.org/ 10.1021/la902679c.
- [59] R. Poetes, K. Holtzmann, K. Franze, U. Steiner, Metastable underwater superhydrophobicity, Phys. Rev. Lett. 105 (2010) 1–4, https://doi.org/10.1103/ PhysRevLett.105.166104.
- [60] M.A. Samaha, H.V. Tafreshi, M. Gad-El-Hak, Influence of flow on longevity of superhydrophobic coatings, Langmuir 28 (2012) 9759–9766, https://doi.org/ 10.1021/la301290e
- [61] P.R. Jones, X. Hao, E.R. Cruz-Chu, K. Rykaczewski, K. Nandy, T.M. Schutzius, K. K. Varanasi, C.M. Megaridis, J.H. Walther, P. Koumoutsakos, H.D. Espinosa, N. A. Patankar, Sustaining dry surfaces under water, Sci. Rep. 5 (2015), 12311, https://doi.org/10.1038/srep12311.
- [62] Y. Lu, S. Sathasivam, J. Song, C.R. Crick, C.J. Carmalt, I.P. Parkin, Robust selfcleaning surfaces that function when exposed to either air or oil, Science 80 (2015) 1132–1135, https://doi.org/10.1126/science.aaa0946.

- [63] H.L. Bai, N. Kevin, J.P. Hutchins, Monty, Turbulence modifications in a turbulent boundary layer over a rough wall with spanwise-alternating roughness strips, Phys. Fluids 30 (2018). https://doi.org/10.1063/1.5026134
- Fluids 30 (2018), https://doi.org/10.1063/1.5026134.

 [64] A. Rajappan, G.H. McKinley, Cooperative drag reduction in turbulent flows using polymer additives and superhydrophobic walls, Phys. Rev. Fluids 5 (2020) 1–18, https://doi.org/10.1103/PhysRevFluids.5.114601.
- [65] M. Nosonovsky, Multiscale roughness and stability of superhydrophobic biomimetic interfaces, Langmuir 23 (2007) 3157–3161, https://doi.org/10.1021/ la062301d.
- [66] S. Heo, W. Choi, S.J. Lee, Enhanced air stability of ridged superhydrophobic surface with nanostructure, AIP Adv. 11 (2021), https://doi.org/10.1063/ E0067770
- [67] T.W.Masashi Miwa, Akira Nakajima, Akira Fujishima, Kazuhito Hashimoto, Effects of the surface roughness on sliding angles of water droplets on superhydrophobic surfaces, Langmuir 16 (2000) 5754–5760, https://doi.org/10.1021/la010847o.